Mol. Cells *27*, 99-103
DOI/10.1007/s10059-009-0010-6

Molecules and Cells

Crystal Structures of Substrate and Inhibitor Complexes of Ribose 5-Phosphate Isomerase A from *Vibrio vulnificus* YJ016

Tae Gyun Kim[1,3], Taek Hun Kwon[2,3], Kyoungin Min[1], Mi-Sook Dong[2], Young In Park[2,*], and Changill Ban[1,*]

Ribose-5-phosphate isomerase A (RpiA) plays an important role in interconverting between ribose-5-phosphate (R5P) and ribulose-5-phosphate in the pentose phosphate pathway and the Calvin cycle. We have determined the crystal structures of the open form RpiA from *Vibrio vulnificus* YJ106 (VvRpiA) in complex with the R5P and the closed form with arabinose-5-phosphate (A5P) in parallel with the apo VvRpiA at 2.0 Å resolution. VvRpiA is highly similar to *Escherichia coli* RpiA, and the VvRpiA-R5P complex strongly resembles the *E. coli* RpiA-A5P complex. Interestingly, unlike the *E. coli* RpiA-A5P complex, the position of A5P in the VvRpiA-A5P complex reveals a different position than the R5P binding mode. VvRpiA-A5P has a sugar ring inside the binding pocket and a phosphate group outside the binding pocket: By contrast, the sugar ring of A5P interacts with the Asp4, Lys7, Ser30, Asp118, and Lys121 residues; the phosphate group of A5P interacts with two water molecules, W51 and W82.

INTRODUCTION

Ribose-5-phosphate isomerase (Rpi; EC 5.3.1.6) is a ubiquitous and highly conserved protein found in prokaryotic and eukaryotic sugar metabolisms (Essenbeg and Cooper, 1975; Hove-Jensen and Maigaard, 1993; Roos, 2007). These metabolisms are involved in the production of NADPH as well as the oxidative and non-oxidative synthesis of pentose sugars (Choquet et al., 1994; Dandekar et al., 1999; Decker et al., 1982; Eisenreich and Bacher, 1991; Melendez-Hevia et al., 1997). Previous results have reported that a deficiency of human Rpi causes the destruction of myelin sheaths in conditions such as leukoencephalopathy and neuronal abnormalities, including peripheral neuropathy (Huck et al., 2004).

Rpi exists as two distinct proteins, RpiA and RpiB, which both catalyze the same reaction, and most organisms express at least one type. The functional and structural properties of RpiA from *Escherichia coli* (Hove-Jensen and Maigaard, 1993; Rangarajan et al., 2002; Zhang et al., 2003), *Pyrococcus horikoshii* (Ishikawa et al., 2002), *Methanocaldococcus jannaschii* (Grochowski et al., 2005), *Thermus thermophilus* (Shin et al., 2003), *Plamodium falciparum* (Holmes et al., 2006), *Saccharomyces cerevisiae* (Graile et al., 2005), and *Spinacia oleracea* (Rault et al., 1993) have been described. The crystal structures of *E. coli* RpiA and its complex with A5P essentially represent the closed conformation with the β-anomer furanose (Rangarajan et al., 2002; Zhang et al., 2003). The crystal structures of *T. thermophilus* RpiA and its complexes with R5P and A5P elucidated the stereospecific isomerization for its ligands, R5P and A5P (Shin et al., 2003). However, until now, the ligand binding and catalyzing mechanisms were not well known.

In this study, we present the crystal structures of RpiA from the pathogenic (Lee et al., 2005; Park et al., 2005) bacterium *Vibrio vulnificus* YJ108 in the apo form at 2.0 Å resolution and in complexes with the open form of R5P and the closed form of A5P. The apo and complex structures allowed us to identify the residues of the active site cleft, particularly showing that the A5P-binding moiety has a different location in VvRpiA in comparison to the *E. coli* RpiA-A5P complex, and thus may reflect an evolutionary adaptation of RpiA to various sugar metabolites.

MATERIALS AND METHODS

Overexpression of *Vibrio vulnificus* YJ016 RpiA

The *rpi*A gene was amplified from *Vibrio vulnificus* YJ016 genomic DNA using gene-specific primers (*rpi*A-forward: 5′-AACGGATCCATGACTCAAGATATGAAAAAAGCC-3′ and *rpi*A-reverse: 5′-AACCTCGAGTTACTCAATTTTGGCGCCTT-3′). The PCR-amplified gene was treated with restriction enzymes (*Bam*HI and *Xho*I in the underlined sequences above, respectively) and then cloned into the *Bam*HI and *Xho*I sites of the bacterial expression vector pET-28aTEV (modified pET-28a (Novagen, Germany) containing a recognition site for Tobacco Etch Virus (TEV) protease) (Heo et al., 2007; Ryu et al., 2007). The construct was verified through automated DNA sequencing. *V. vulnificus* RpiA (VvRpiA) was overexpressed in BL21(DE3) cells (Invitrogen, USA) in two liters of Luria-Bertani medium containing 50 μg/ml kanamycin at 37°C. When the absorbance

[1]Department of Chemistry, Pohang University of Science and Technology, Pohang 790-784, Korea, [2]School of Life Sciences and Biotechnology, Korea University, Seoul 136-701, Korea, [3]These authors equally contributed to this work.
*Correspondence: yipark@korea.ac.kr (YIP), ciban@postech.ac.kr (CB)

Received October 21, 2008; accepted October 28, 2008; published online February 5, 2009

Keywords: Arabinose-5-phosphate, crystal structure, *E. coli* RpiA, Ribose-5-phosphate isomerase A (RpiA), *Vibrio vulnificus* YJ016

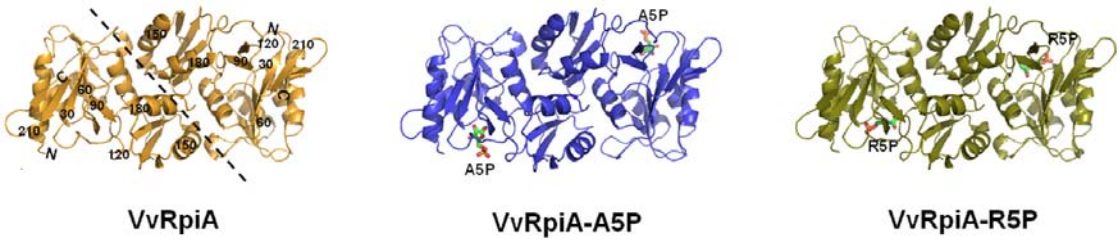

Fig. 1. Ribbon diagrams of the overall structure of VvRpiA and its complexes with the inhibitor arabinose-5-phosphate (A5P, blue) and the substrate ribose-5-phosphate (R5P, olive). The numbers and dashed line indicate the residue numbers and pseudo two-fold symmetry, respectively.

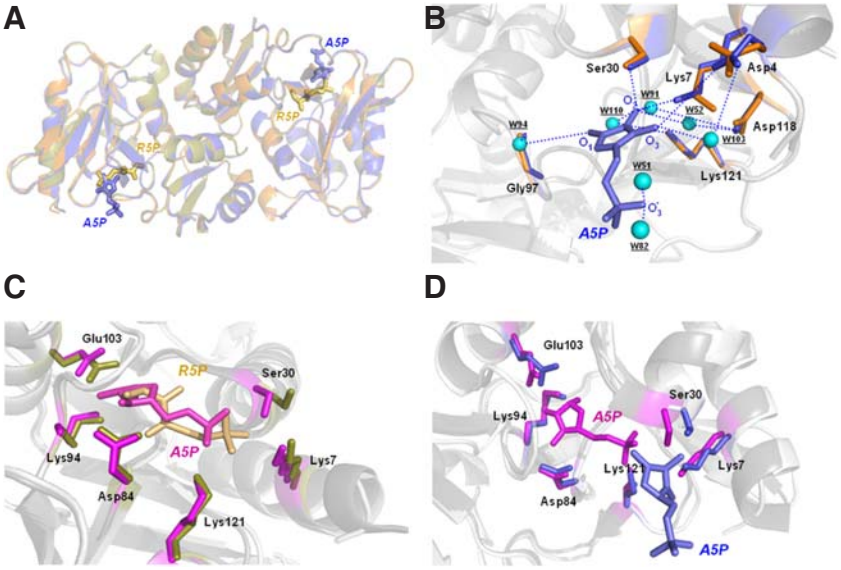

Fig. 2. Superimposed representations of VvRpiA, *E. coli* RpiA, and their complexes with A5P and R5P. (A) Superimposed representation of VvRpiA and its complexes with A5P and R5P. The orange, blue, and olive colors represent VvRpiA, VvRpiA-A5P, and VvRpiA-R5P, respectively. (B) Superimposition of VvRpiA and the VvRpiA-A5P complex in the last refinement cycle. O_1, O_2, and O_3 are the oxygens of the pentose sugar ring of A5P. O'_3 is the oxygen of the phosphate group of A5P. The orange and blue colors highlight the indicated residues of VvRpiA and VvRpiA-A5P, respectively. The blue dotted lines show the interactions between atoms. W (cyan) indicates the water molecules. (C) is a similar coordination between the VvRpiA-R5P and *E. coli* RpiA-A5P complexes. The indicated residues of *E. coli* RpiA-A5P and A5P are colored in magenta, and the residues of VvRpiA-R5P and R5P are olive and light orange, respectively. (D) is a different coordination between the VvRpiA-A5P and *E. coli* RpiA-A5P complexes. The residues of *E. coli* RpiA-A5P and A5P (magenta) and of VvRpiA-A5P and A5P (blue) are highlighted.

at 600 nm reached 0.6, expression was induced by the addition of 0.3 mM isopropyl-thiogalactopyranoside (IPTG) for 12 h at 20°C. Cells were harvested by centrifugation, resuspended in lysis buffer [20 mM Tris-HCl, pH = 8.0, 500 mM NaCl, 0.5 mM β-mercaptoethanol, and EDTA-free protease inhibitor tablet (Roche Applied Science)], and disrupted by sonication. The lysate was centrifuged at 25,000 × *g* for 30 min at 4°C, and the supernatant was used in subsequent experiments.

Purification of VvRpiA

After filtration of the sample, supernatants were applied to a nickel-nitrilotriacetic acid (Ni-NTA, GE Healthcare, Denmark) affinity column pre-equilibrated with a 100 mM $NiCl_2$ solution and buffer I [lysis buffer with 5% (v/v) glycerol and 5 mM imidazole]. His-tagged VvRpiA was eluted with elution buffer [buffer I with 5% (v/v) glycerol and 300 mM imidazole]. His-tagged fragments of VvRpiA were cleaved by TEV protease at room temperature for 10 h. To remove uncleaved His-tagged VvRpiA and cleaved His-tag fragments, samples were re-loaded onto the Ni-NTA affinity column, and the target protein was collected in the flow-through. For further purification, VvRpiA was loaded onto a DEAE anion exchange column (GE Healthcare, Denmark) equilibrated with buffer II [20 mM Tris-HCl, pH 8.0, 500 mM NaCl, 1 mM dithiothreitol (DTT), 0.5 mM EDTA, 5% (v/v) glycerol, and 1 mM ethylenediaminetetraacetic acid (EDTA)] and eluted in buffer II with a linear gradient of 0.5 M NaCl. Based on the isoelectric point (4.77), VvRpiA was applied to a weak DEAE anion exchange column and then eluted between 250 to 275 mM NaCl. After concentration using Ultracell-5K concentrators (Millipore, USA), VvRpiA was finally purified using a Superdex 75 HR gel filtration column (GE Healthcare, Denmark) equilibrated with buffer III (20 mM HEPES (pH 7.5), 150 mM KCl, 10% (v/v) glycerol and 10 mM β-mercaptoethanol). The purified VvRpiA was concentrated and then analyzed by sodium dodecylsulfate polyacrylamide gel electrophoresis (SDS-PAGE). We identified a band with a molecular weight of less than 25 kDa, which is consistent with the theoretically calculated size of 24 kDa (Supplementary Fig. 1A). For the determination of protein concentration, a Cary 400 spectrophotometer (VARIAN) and theoretical extinction coefficient for VvRpiA (13075 M^{-1} cm^{-1}, wild-type) were used.

Analytical size exclusion chromatography

The native molecular weight of VvRpiA was determined by chromatography with a Superdex 75HL column equilibrated with buffer III at 4°C with a flow rate of 0.5 ml/min. All samples were loaded into a 0.5 ml injection loop. The elution of a protein can be described in terms of its corresponding K_{av} value, $K_{av} = (V_e-V_o)/(V_t-V_o)$, where V_e is the elution volume of the particular molecule, V_o is the void volume of the column and V_t is the total bed volume. Molecular weight standard proteins (Sigma), bovine serum albumin (BSA, 66 kDa in monomer), ovalbumin (43 kDa),

Table 1. Data collection and refinement statistics

Data details	Native (VvRpiA)	Substrate (VvRpiA-R5P)	Inhibitor (VvRpiA-A5P)
Space group	R3	R3	R3
Unit cell parameters (Å)	77.094 77.094 189.995 90.000 90.000 120.000	77.062 77.062 189.258 90.000 90.000 120.000	77.022 77.022 190.294 90.000 90.000 120.000
Observations	678201	679102	319267
Resolution range (Å)	50.0-1.49 (1.54-1.49)	50.0-1.5 (1.55-1.50)	50.0-2.00 (2.07-2.00)
Number of reflections	68818	64147	28467
Completeness (%)	99.6 (97.5)	95.0 (74.5)	100.0 (100.0)
I/σ (I)	8.8	17.1	11.7
R_{merge}[a] (%)	8.6 (15.3)	6.4 (38.2)	10.3 (32.9)
Redundancy	10.3	10.6	11.2
Refinement statistics			
Resolution range[b] (Å)	25.0-2.0	32.9-2.0	33.0-2.0
Completeness (% total)	99.90	99.90	99.00
R_{work}[c] (%)	22.12	20.98	23.94
R_{free}[d] (%)	27.15	25.61	30.95
Stereochemical parameters			
Bond length (RMS observed) (Å)	0.007	0.005	0.008
Bond angle (RMS observed) (deg.)	1.109	0.988	1.140

[a] $R_{merge} = \Sigma|I_{obs} - I_{avg}|/\Sigma I_{avg}$
[b] Refinement was performed with data collected at 1.0 Å
[c] $R_{work} = \Sigma|F_{obs} - F_{calc}|/\Sigma F_{obs}$
[d] $R_{free} = R_{work}$, except for a random set of 10% of the unique reflections
Values in parentheses refer to the highest resolution shell

α-chymotrypsin (25 kDa), and ribonuclease A (13.7 kDa), were used for size calibrations. Sequence alignment was performed with CLUSTALW (Thompson et al., 1994) and ESPRIPT (Gouet et al., 2003).

Dynamic light scattering

Dynamic light scattering (DLS) measurements were carried out to determine the size distribution of the purified VvRpiA (100 μM). The mean peak value was taken as the apparent hydrodynamic radius of the target protein as determined by an automated program. The mean hydrodynamic diameter (*d*) was estimated using the Debye-Einstein-Stokes equation, $D = k_B T/6\pi\eta r$ (k_B is the Boltzmann constant, T is the absolute temperature, η is the viscosity of the dispersing medium, and D is the apparent diffusion coefficient).

Crystallization of VvRpiA and its complexes with substrate and inhibitor

The hanging drop vapor diffusion method (Lim et al., 2008) was used for the crystallization of VvRpiA. Two microliters of a VvRpiA solution (30 mg/ml in 20 mM HEPES, pH 7.5 and 150 mM KCl) was mixed with 2 μl of a reservoir solution (50 mM succinate, pH 4.1, 180 mM ammonium sulfate, and 8% 4K PEG). The initial screenings were able to reproduce apo VvRpiA crystals under 30 mg/mL within three days at 20°C. VvRpiA-R5P and -A5P complexes were co-crystallized at the same ratio of protein solution (30 mg/ml in 20 mM HEPES, pH 7.5, 50 to 150 mM KCl, and 20 mM R5P and A5P) to reservoir solution. Co-crystallizations between VvRpiA and R5P/A5P were performed at 20°C for three days. The crystals could be directly flash-frozen with the addition of a cryoprotectant solution, an important step for improving the diffraction quality of the crystals. To optimize the cryoprotectant, we used 30% (v/v) glycerol in addition to the buffers (VvRpiA: 50 mM succinate, pH 4.1, 180 mM ammonium sulfate, and 8% 4K PEG; VvRpiA-A5P: 50 mM succinate, pH 4.1, 180 mM ammonium sulfate, 8% 4K PEG, and 20 mM arabinose-5-phosphate; VvRpiA-R5P: 50 mM succinate, pH 4.1, 180 mM ammonium sulfate, 8% 4K PEG, and 20 mM ribose-5-phosphate). To confirm the crystals of VvRpiA and its complexes with R5P and A5P, crystals were color-verified with Izit Crystal Dye™ (Hampton Research).

X-ray data collection and processing

Crystals remained in the cryogenic solution for approximate 30 min and were then flash-frozen through a cold nitrogen stream for data collection. Diffraction X-ray data for VvRpiA crystals and the complex crystals (VvRpiA-A5P and VvRpiA-R5P) were collected at 100K at the 4A beamline of the High Flux Macromolecular Crystallography at the Pohang Accelerator Laboratory. A 1° oscillation (up to 360°) and a crystal-to-detector distance of 150 mm were used. The data were integrated and scaled with *HKL*2000 (Otwinowski and Minor, 1997) and Mosflm (Leslie, 1999). More details on data collection are shown in Table 1.

Structure determination and refinement

Phasing was done with molecular replacement using the CCP4i suite. Map conversion was performed using xdlmapman in the Uppsala Software Factory (http://xray.bmc.uu.se/usf/). All

model building was performed with COOT and refined with CNS (Brunger et al., 1998) and PHENIX ver. 1.3 (Adams et al., 2002). Water picking was carried out with PHENIX using default parameters. The stereochemistry of the structure was assessed with PROCHECK (Laskowski et al., 1993), and a stringent boundary Ramachandran plot (Kleywegt and Jones, 1996) showed the residual allowances of the models. All figures for the structural model were made in PyMol (DeLano, 2002). The data collection and refinement statistics are summarized in Table 1.

RESULTS AND DISCUSSION

Characterization of VvRpiA

Preliminary purification of VvRpiA was conducted using optimizing buffers such as 20 mM Tris-HCl (pH 8.0) and 50 mM sodium phosphate (pH 7.5). However, the purified VvRpiA showed some instability, such as precipitation at low salt concentrations and aggregation during crystallization. VvRpiA (24 kDa monomer, Supplementary Fig. 1A), which proved to be stable in buffer III, was loaded onto a Superdex 75 HR column to determine the oligomeric state of the native protein. The FPLC trace showed only one peak, which ranged from 40 to 50 kDa, corresponding to the dimeric form of VvRpiA, and no peak was observed for the aggregated form (Supplementary Fig. 1B). *E. coli* RpiA was partially purified previously, and the gel filtration results revealed a molecular weight of the native enzyme of 45 kDa. In comparison with our determination of a subunit molecular weight of 20 to 25 kDa, it appears that the enzyme is composed of two subunits of equal size. To further elucidate the homogeneity and structural stability of VvRpiA, DLS measurements were obtained. DLS results showed a high purity of VvRpiA with only one peak ranging from 1 nm to 10,000 nm (Supplementary Fig. 2), suggesting that our preparation was free of the aggregated form.

Overall structure of dimeric VvRpiA

The crystallizations were optimized to form primitive rhombohedral crystals (Supplementary Fig. 1B, inset). The 2.5 Å structure of apo VvRpiA was determined from a single crystal of VvRpiA based on the *E. coli* RpiA structure (PDB ID: 108B (Rangarajan et al., 2002; Zhang et al., 2003)) using the molecular replacement method. The VvRpiA-A5P and VvRpiA-R5P complex structures were subsequently refined at 2.0 Å, as shown in Table 1.

Apo VvRpiA and its complexes with A5P and R5P all include three β-sheets, onto which a total of six α-helices are compacted (Fig. 1). Electron-dense patches could be clearly observed. Residues 2 to 218 in subunits A and B of VvRpiA, VvRpiA-A5P and VvRpiA-R5P were defined as the ordered regions. The electron density maps showed the presence of electron-dense regions that could be modeled in each subunit. The models corresponding to the complete monomers were transferred to high-resolution data.

VvRpiA appears in the crystal as a dimer with a pseudo twofold symmetry (Fig. 1, left), in agreement with known results for *E. coli* (Zhang et al., 2003) and other enzymes (Ishikawa et al., 2002; Shin et al., 2003; Rault et al., 1993). The dimer interface between the two subunits is stabilized by hydrophobic interactions and water-associated hydrogen bonds from several regions of each subunit: Cys70-Ser75 near η2, Thr101-Ile109 in α4, Ile136-Arg145 in η2, Asn164/Asn166 in the random coil before β8, and Asp184/Asn187/Ala188/Pro190-Val193 near α6 and a turn region. Chain tracing was performed on one of the monomers. The initially drawn model of VvRpiA was then used to find the position of the other monomer in the asymmetric unit.

Sequence alignment analysis between VvRpiA and known RpiAs revealed structural conservation with sequential similarity (Supplementary Fig. 3). In particular, the previously determined *E. coli* RpiA structure shares approximately 75% sequence identity with the VvRpiA structure. In addition, superimpositions of VvRpiA and other RpiA structures (*M. jannaschii* [from PDB ID: 2PJM deposited data] and *S. cerevisiae* RpiAs (Graile et al., 2005)) showed similarly overlapping structures (Supplementary Fig. 4). Although the substrate-binding regions and dimer interface of VvRpiA are highly conserved in the sequence alignment, the inhibitor-interacting regions are located at slightly different residues compared to the *E. coli* RpiA amino acid sequences (Fig. 2).

The binding mode of inhibitor and substrate

Arabinose-5-phosphate (A5P) and ribose-5-phosphate (R5P) are an inhibitor and a substrate, respectively, for *E. coli* RpiA (Rangarajan et al., 2002; Zhang et al., 2003). The superimposed models of VvRpiA, VvRpiA-A5P, and VvRpiA-R5P show that these structures belong to the same space group, R3 (Fig. 2A). As depicted in Figure 2B, A5P interacts with several regions of one subunit. The O_2 of A5P directly interacts with Lys7, Ser30, and Asp118; the O_3 of A5P directly interacts with Asp4; the O_1 of A5P interacts with W94 (water 94); the O'_3 of A5P interacts with W51 and W82; the O_2 of A5P distantly interacts with Asp118 and Lys121 via W110 and W52/91, respectively; and the O_3 of A5P interacts with Asp4 via W103. This A5P has a sugar ring in the binding pocket and a phosphate group outside of it. The superimposition of the VvRpiA-R5P and *E. coli* RpiA-A5P complexes revealed the sequence conservation in the active site, which is composed of amino acid residues such as Lys7, Ser30, Asp84, Lys94, Glu103, and Lys121 (Fig. 2C). Interestingly, as seen in Fig. 2D, we determined the proximal distance between A5P and R5P to be approximately 10 Å. In the VvRpiA-A5P complex, A5P is located at the opening of the active site, mainly through the attractive interaction between O_2 and Lys7 and a slight repulsion of Ser30 from O_2 (Figs. 2B and 2D). Lys7 of VvRpiA undergoes the most dramatic change when A5P approaches the active site. In addition, the root mean square deviation (RMSD) values, 0.464, 0.736, and 0.781 Å, were calculated for VvRpiA to VvRpiA-A5P, VvRpiA to *E. coli* RpiA, and VvRpiA-A5P to *E. coli* RpiA-A5P, respectively (Supplementary Fig. 5). Despite the high sequence similarity between VvRpiA and *E. coli* RpiA, the RMSD values reveal that the overall Cα atoms have considerably different locations in the VvRpiA and *E. coli* RpiA structures.

Biological implications

RpiA plays an important role in producing nucleotides and cofactors from ribose-5-phosphate in the pentose phosphate pathway and the Calvin cycle in plants. The sequence conservation among RpiA subfamilies denotes that there is considerable evolutionary significance in preserving the VvRpiA structure, especially with a different coordination site of structural polarization for the inhibitor A5P. The recent emergence of pathogenic bacteria that are resistant to current antibiotic treatments has prompted a renewed interest in the identification of novel molecular targets for antibacterial inhibitors, which may be of use for the treatment of abnormal symptoms resulting from unbalanced cellular ribose levels.

Protein data bank codes

The atomic coordinates and structural factors for VvRpiA (PDB ID: 3ENQ), VvRpiA-R5P (PDB ID: 3ENW), and VvRpiA-A5P

(PDB ID: 3ENV) were deposited in the Protein Data Bank, Research Collaboratory for Structural Bioinformatics, Rutgers University, New Brunswick, NJ (http://www.rcsb.org/).

Note: Supplementary information is available on the Molecules and Cells website (www.molcells.org).

ACKNOWLEDGMENTS

This work was supported by grants from the Korea Science and Engineering Foundation through the Center for Integrated Molecular System at Pohang University of Science and Technology (grant number: R11-2000-070-070010), the Korea Health Industry Development Institute (grant number: A020605), the Korea Health Industry Development Institute through the Healthcare and Biotechnology Development Program (grant number: A050426) and the Korea Research Foundation Grant (KRF-2008-314-C00218).

REFERENCES

Adams, P.D., Grosse-Kunstleve, R.W., Hung, L.W., Ioerger, T.R., McCoy, A.J., Moriarty, N.W., Read, R.J., Sacchettini, J.C., Sauter, N.K., and Terwilliger, T.C. (2002). PHENIX: building new software for automated crystallographic structure determination. Acta Crystallogr. *D58*, 1948-1954.

Brunger, A.T., Adams, P.D., Clore, G.M., Delano, W.L., Gros, P., Grosse-Kunsteve, R.W., Jiang, J.S., Kuszwewski, J., Nilges, M., and Pannu, N.S. (1998). Crystallography & NMR system: a new software suite for macromolecular structure determination. Acta Crystallogr. *D54*, 905-921.

Choquet, C.G., Richards, J.C., Patel, G.B., and Sprott, G.D. (1994). Ribose biosynthesis in methanogenic bacteria. Arch. Microbiol. *161*, 481-488.

Dandekar, T., Schuster, S., Snel, B., Huyen, M., and Bork, P. (1999). Pathway alignment: application to the comparative analysis of glycolytic enzymes. Biochem. J. *343*, 115-124.

Decker, P., Schweer, H., and Pohlmann, R. (1982). Identification of formose sugars, presumable prebiotic metabolites, using capillary gas chromatography/gas chromatography-mass spectrometry of *n*-butoximine trifluoroactatcs on OV-225. J. Chromatogr. *244*, 281-291.

DeLano, W.L. (2002). The PyMOL Molecular Graphics System, DeLano Scientific, San Carlos, CA.

Eisenreich, W., and Bacher, A. (1991). Biosynthesis of 5-hydroxybenzimidazolycobamid (factor III) in *Methanobacterium thermoautotrophicum*. J. Biol. Chem. *266*, 23840-23849.

Essenbeg, M.K., and Cooper, R.A. (1975). Two ribose-5-phosphate isomerases from *Escherichia coli* K-12: partial characterization of the enzymes and consideration of their possible physiological roles. Eur. J. Biochem. *55*, 323-332.

Gouet, P., Robert, X., and Courcelle, E. (2003). ESPript/ENDscript: extracting and rendering sequence and 3D information from atomic structures of proteins. Nucleic Acids Res. *31*, 3320-3323.

Graile, M., Meyer, P., Leulloit, N., Sorel, I., Janin, J., Van Tilbeurgh, H., and Quevillon-Cheruel, S. (2005). Crystal structure of the *S. cerevisiae* D-ribose-5-phosphate isomerase: comparison with the archaeal and bacterial enzymes. Biochimie *87*, 763-769.

Grochowski, L.L., Xu, H., and White, R.H. (2005). Ribose-5-phosphate biosynthesis in *Methanocaldococcus jannaschii* Occurs in the absence of pentose-phosphate pathway. J. Bacteriol. *187*, 7382-7389.

Heo, S.D., Cho, M., Ku, J.K., and Ban, C. (2007). Steady-state ATPase activity of *E. coli* MutS modulated by its dissociation from heteroduplex DNA. Biochem. Biophys. Res. Commun. *364*, 264-269.

Holmes, M.A., Buckner, F.S., Van Voorhis, W.C., Verlinde, C.L.M.J., Mehlin, C., Boni, E., DeTitta, G., Luft, J., Lauricella, A., Anderson, L., et al. (2006). Structure of ribose 5-phosphate isomerase from *Plasmodium falciparum*. Acta Crystallogr. *F62*, 427-431.

Hove-Jensen, B., and Maigaard, M. (1993). *Escherichia coli rpiA* gene encoding ribose phosphate isomerase A. J. Bacteriol. *175*, 5628-5635.

Huck, J.H., Verhoeven, N.M., Struys, E.A., Salomons, G.S., Jakobs, C., and van der Knaap, M.S. (2004). Ribose-5-phosphate isomerase deficiency: new inborn error in the pentose phosphate pathway associated with a slowly progrssive leukoencephalopathy. Am. J. Hum. Genet. *74*, 745-751.

Ishikawa, K., Matsui, I., Payan, F., Cambillau, C., Ishida, H., Kawarabayasi, Y., Kikuchi, H., and Roussel, A. (2002). A hyperthermostable D-ribose-5-phosphate isomerase from *Pyrococcus horikoshii* characterization and three-dimensional structure. Structure *10*, 877-886.

Kleywegt, G.J., and Jones, T.A. (1996). Phi/psi-chology: Ramachandran revisited. Structure *4*, 1395-1400.

Laskowski, R.A., Macarthur, M.W., Moss, D.S., and Thornton, J.M. (1993). PROCHECK: a program to check the stereochemical quality of the protein structure. J. Appl. Crystallogr. *26*, 283-291.

Lee, J.H., Kim, S.Y., Rho, S.-H., Im, Y.J., Kim, Y.R., Kim, M.-K., Kang, G.B., Rhee, J.H., and Eom, S.H. (2005). Crystallization and preliminary X-ray crystallographic analysis of PAS factor from *Vibrio vulnificus*. Mol. Cells *20*, 361-363.

Leslie, A.G. (1999). Integration of macromolecular diffraction data. Acta Crystallogr. D. Biol. Crystallogr. *55*, 1696-1702.

Lim, H., Kim, K., Han, D., Oh, J., and Kim, Y. (2008). Crystal Structure of TTC0263, a Thermophilic TPR Protein from *Thermus thermophilus* HB27. Mol. Cells *24*, 27-36.

Melendez-Hevia, E., Waddell, T.G., Heinrich, R., and Montero, F. (1997). Theoretical approaches to the evolutionary optimization of glycolysis-chemical analysis. Eur. J. Biochem. *244*, 527-543.

Otwinowski, Z. and Minor, W. (1997). Processing of x-ray diffraction data collected in oscillation mode. Methods Enzymol. *276*, 307-326.

Park, S.-Y., Heo, Y.-J., Kim, K.-S., and Cho, Y.-H. (2005). *Drosophila melanogaster* Is Susceptible to *Vibrio cholerae* Infection. Mol. Cells *20*, 409-415.

Rangarajan, E.S., Sivaraman, J., Matte, A., and Cygler, M. (2002). Crystal structure of D-ribose-5-phosphate isomerase (RpiA) from *Escherichia coli*. PROTEINS: Structure, Functions, and Genetics *48*, 737-740.

Rault, M., Giudici-Orticoni, M.T., Gontero, B., and Ricard, J. (1993). Structural and functional properties of a multi-enzyme complex from spinach chloroplast. 1. Stoichiometry of the polypeptide chains. Eur. J. Biochem. *217*, 1065-1073.

Roos, A.K. (2007). Structural and Functional Studies of Ribose-5-phosphate isomerase B. Digital Comprehensive Summaries of Uppsala Dissertations from the Faculty of Science and Technology *332*, 1-5.

Ryu, E.K., Kim, T.G., Kwon, T.H., Jung, I.D., Ryu, D., Park, Y.M., Kim, J., Ahn, K.H., and Ban, C. (2007). Crystal structure of recombinant human stromal cell-derived factor-1α. PROTEINS: Structure, Function, and Bioinformatics *67*, 1193-1197.

Shin, D.H., Roberts, A., Jancarik, J., Yokota, H., Kim, R., Wemmer, D.E., and Kim, S.H. (2003). Crystal structure of a phosphatase with a unique substrate binding domain from *Thermotoga maritime*. Protein Sci. *12*, 1464-1472.

Thompson, J.D., Higgins, D.G., and Gibson, T.J. (1994). CLUSTAL W: improving the sensitivity of progressive multiple sequence alignment through sequence weighting, position-specific gap penalties and weight matrix choice. Nucleic Acids Res. *22*, 4673-4680.

Zhang, R., Andersson, C.E., Savchenko, A., Skarina, T., Evdokimova, E., Beasley, S., Arrowsmith, C.H., Edwards, A.M., Joachimiak, A., and Mowbray, S.L. (2003). Structure of *Escherichia coli* ribose-5-phosphate isomerase: a ubiquitous enzyme of the pentose phosphate pathway and the Calvin cycle. Structure *11*, 31-42.